NACA

RESEARCH MEMORANDUM

AERODYNAMIC CHARACTERISTICS OF A WING WITH QUARTER-CHORD LINE SWEPT BACK 45°, ASPECT RATIO 6, TAPER RATIO 0.6, AND NACA 65A009 AIRFOIL SECTION

TRANSONIC-BUMP METHOD

By Kenneth P. Spreemann, William D. Morrison, Jr.,
and Thomas B. Pasteur, Jr.

Langley Aeronautical Laboratory
Langley Air Force Base, Va.

NATIONAL ADVISORY COMMITTEE
FOR AERONAUTICS

WASHINGTON

April 6, 1950

NACA RM L50B03a

NATIONAL ADVISORY COMMITTEE FOR AERONAUTICS

RESEARCH MEMORANDUM

AERODYNAMIC CHARACTERISTICS OF A WING WITH QUARTER-CHORD LINE SWEPT BACK 45°, ASPECT RATIO 6, TAPER RATIO 0.6, AND NACA 65A009 AIRFOIL SECTION

TRANSONIC-BUMP METHOD

By Kenneth P. Spreemann, William D. Morrison, Jr.,
and Thomas B. Pasteur, Jr.

SUMMARY

As part of a transonic research program, a series of wings are being investigated in the Langley high-speed 7- by 10-foot tunnel over a Mach number range of approximately 0.60 to 1.18 by use of the transonic-bump test technique.

This paper presents the results of the investigation of a wing-alone and wing-fuselage configurations employing a wing with the quarter-chord line swept back 45°, aspect ratio 6, taper ratio 0.6, and an NACA 65A009 airfoil section. Lift, drag, pitching moment, and root bending moment were obtained for these configurations. In addition, effective downwash angles and dynamic-pressure characteristics in the region of probable tail locations were obtained for these configurations and are presented for a range of tail heights at one tail length.

INTRODUCTION

A series of wings are being investigated in the Langley high-speed 7- by 10-foot tunnel to study the effects of wing geometry on the wing-alone and wing-fuselage longitudinal stability characteristics at transonic speeds. For correlation purposes the same fuselage is being used for all wings tested. A Mach number range between 0.60 and 1.18 is obtained by use of the transonic-bump technique.

This paper presents the results of the investigation of the wing-alone and wing-fuselage configurations employing a wing with the quarter-chord line swept back 45°, aspect ratio 6, taper ratio 0.6, and an NACA 65A009 airfoil section parallel to the air stream. In order to expedite the publishing of these data, only a brief analysis is included. Previous data published in this series for wings incorporating 45° sweepback can be obtained in references 1 to 3.

MODEL AND APPARATUS

The wing of the semispan model had 45° of sweepback referred to the quarter-chord line, aspect ratio 6, taper ratio 0.6, and an NACA 65A009 airfoil section parallel to the free stream. A two-view drawing of the model is presented in figure 1 and ordinates of the fuselage of actual fineness ratio 10 (and basic fineness ratio 12) are given in table I. The wing was made of beryllium copper and the fuselage, of brass.

The model was mounted on an electrical strain-gage balance enclosed in the bump. The lift, drag, pitching moment, and root bending moment were measured with the aid of galvanometers. The angle of attack was measured by means of a slide-wire potentiometer and recorded with the aid of a galvanometer.

Effective downwash angles were determined for a range of tail heights, at a representative tail length of 86 percent of the semispan, by measuring the floating angles of five geometrically similar free-floating tails with the aid of calibrated slide-wire potentiometers. Details of the floating tails are shown in figures 2 and 3 and a photograph of the model on the bump with three of the floating tails is shown as figure 4. The tails used in this investigation were the same as those used in references 1 to 3. A pictorial view showing the sponge-wiper seal installed on the model is given as figure 5.

A total-pressure rake was used to determine point dynamic-pressure ratios for a range of tail heights in a plane which contained the 25-percent mean-aerodynamic-chord point of the free-floating tails. The total-pressure tubes were spaced 0.125 inch apart for a distance of 1.0 inch below and 0.5 inch above the wing chord plane extended ($\alpha = 0°$) and 0.25 inch apart over the remainder of the rake.

[redacted]

COEFFICIENT AND SYMBOLS

C_L lift coefficient $\left(\frac{\text{Twice semispan lift}}{qS}\right)$

C_D drag coefficient $\left(\frac{\text{Twice semispan drag}}{qS}\right)$

C_m pitching-moment coefficient referred to $0.25\bar{c}$ $\left(\frac{\text{Twice semispan pitching moment}}{qS\bar{c}}\right)$

C_B bending-moment coefficient at plane of symmetry $\left(\frac{\text{Root bending moment}}{q\frac{S}{2}\frac{b}{2}}\right)$

q effective dynamic pressure over span of model, pounds per square foot $\left(\frac{1}{2}\rho V^2\right)$

q_a average chordwise local dynamic pressure

S twice wing area of semispan model, 0.125 square foot

$\bar{c}$ mean aerodynamic chord of wing, 0.147 foot; based on relationship $\frac{2}{S}\int_0^{b/2} c^2 dy$ (using theoretical tip)

$\bar{c}_t$ mean aerodynamic chord of tail, 0.0667 foot

c local wing chord

b twice span of semispan model, 0.866 foot

y spanwise distance from plane of symmetry

ρ air density, slugs per cubic foot

[redacted]

V	free-stream velocity, feet per second
M	effective Mach number over span of model
M_l	local Mach number
M_a	average chordwise local Mach number
R	Reynolds number of wing based on $\bar{c}$
α	angle of attack, relative to the wing chord line, degrees
ϵ	effective downwash angle, degrees
$\frac{q_{wake}}{q}$	ratio of point dynamic pressure, taken along a line containing quarter-chord points of mean aerodynamic chords of free-floating tails, to local free-stream dynamic pressure
y_{cp}	lateral center of pressure, percent semispan ($100\ C_B/C_L$)
h_t	tail height relative to wing chord plane extended, percent wing semispan; positive for tail positions above wing chord plane extended

TESTS

The tests were conducted in the Langley high-speed 7- by 10-foot tunnel utilizing an adaptation of the NACA wing-flow technique for obtaining transonic speeds. This technique involves the mounting of a model in the high-velocity flow field generated over the curved surface of a bump located on the tunnel floor (reference 4).

Typical contours of local Mach number in the vicinity of the model location on the bump, obtained from surveys with no model in position, are shown in figure 6. It is seen that there is a Mach number variation of about 0.05 over the model semispan at the lowest Mach numbers and from 0.08 to 0.09 at the highest Mach numbers. The chordwise Mach number variation is generally less than 0.01. No attempt has been made to evaluate the effects of the chordwise and spanwise Mach number variations. The long-dashed lines near the root of the wing (fig. 6) represent a local Mach number that is 5 percent below the maximum value and indicate

[redacted]

the extent of the bump boundary layer. The effective test Mach number was obtained from contour charts similar to those presented in figure 6 using the relationship

$$M = \frac{2}{S}\int_0^{b/2} cM_a \, dy$$

Similarly the effective dynamic pressure was determined from dynamic-pressure contour charts by using the relation

$$q = \frac{2}{S}\int_0^{b/2} cq_a \, dy$$

The variation of mean test Reynolds number with Mach number is shown in figure 7. The boundaries on the figure indicate the range in Reynolds number caused by variations in atmospheric test conditions in the course of the investigation.

Force and moment data, effective downwash angles, and the ratio of dynamic pressure at 25 percent of the tail mean aerodynamic chord to free-stream dynamic pressure were obtained for the model configurations tested through a Mach number range of 0.60 to 1.18 and an angle-of-attack range of -4° to 10°.

The end-plate tare corrections to the drag and to the downwash data were obtained through the test Mach number range at an angle of attack of 0° by testing the model configurations without end plates. The results of the end-plate tares of previous investigations were found to be constant with angle of attack and the tares obtained at zero angle of attack in the present investigation were applied to all drag and downwash data. No end-plate tare corrections were applied to the bending moments. A gap of about 1/16 inch was maintained between the wing root chord and the bump surface and a sponge-wiper seal (fig. 5) was fastened to the wing butt beneath the surface of the bump to minimize leakage. Jet-boundary corrections have not been evaluated because the boundary conditions to be satisfied are not rigorously defined. However, inasmuch as the effective flow field is large compared with the span and chord of the model the corrections are believed to be small. No base pressure correction has been applied to the wing-fuselage drag data.

[redacted]

By measuring tail floating angles without a model installed it was determined that a tail spacing of 2 inches would produce negligible interference effects of reflected shock waves on the tail floating angles. Downwash angles for the wing-alone configuration were therefore obtained simultaneously for the middle, highest, and lowest tail positions in one series of tests and simultaneously for the two intermediate positions in succeeding runs. Excluding the middle tail, the same procedure was used to determine the effective downwash angles for the wing-fuselage configuration. In order to obtain downwash data for the chord-plane-extended position, a series of tests were made with a free-floating tail mounted on the center line of the fuselage. The downwash angles presented are increments from the tail floating angles without the model installed. It should be noted that the floating angles measured are in reality a measure of the angle of zero pitching moment about the tail-pivot axis rather than the angle of zero lift. Inasmuch as a spanwise gradient would introduce errors in the measured downwash angle, it has been estimated that for this tail arrangement a linear downwash gradient as large as 2° across the span of the tail will result in an error of 0.2°.

The total-pressure readings in the tail plane were obtained at constant angles of attack through the Mach number range without an end plate on the model to eliminate end-plate wakes and with the support strut gap sealed with a rubber-sponge type of seal to minimize strut leakage effects. The static-pressure values used in computing dynamic-pressure ratios were obtained by use of a static probe without a model in position.

RESULTS AND DISCUSSION

A list of the figures presenting the results follows:

Unless otherwise noted, the discussion is based on the summary curves presented in figure 14. The slopes presented in this figure have been averaged over a lift-coefficient range of ± 0.1 of the specified lift coefficient.

[redacted]

Lift and Drag Characteristics

The wing-alone lift-curve slope $\left(\partial C_L/\partial \alpha\right)_M$ measured near zero lift was about 0.057 at a Mach number of 0.60. This slope compared with a value of 0.062 estimated for this Mach number using the low-speed data of reference 5 ($R = 1.5 \times 10^6$ to 6.0×10^6) for a 6-percent-thick wing of identical plan form applying the three-dimensional Prandtl-Glauert correction to account for the compressibility effects. The lift-curve slope was practically invariant with Mach number below force break and was about the same as the results of a 6-percent-thick wing of identical plan form reported in reference 3 up to $M = 0.95$ and above $M = 1.06$. However, between $M = 0.95$ and 1.06 the lift-curve slope was appreciably less for the 9-percent-thick wing of the present investigation. The addition of the fuselage increased the lift-curve slope approximately 0.007 throughout the test Mach number range.

At a Mach number of 1.10 the drag coefficient for the wing alone at $C_L = 0$ and 0.4 was 0.032 and 0.068, respectively (see fig. 8). Corresponding values of C_D of 0.022 and 0.042 obtained from reference 3 clearly indicate the value of decreasing the wing thickness on the performance characteristics at supersonic speeds.

The lateral center of pressure y_{cp} for the wing alone was located at about 45 percent of the semispan between Mach numbers of 0.60 and 0.90 at lift coefficients below 0.2 (see fig. 8). The same value of y_{cp} was obtained for the 6-percent-thick wing at low speeds and higher Reynolds numbers (reference 5), and throughout the subsonic speed range at the same Reynolds number (reference 3). For Mach numbers near 1.0 and at low lift coefficients the center of pressure moved inboard appreciably (see figs. 8 and 14). This shift of y_{cp} was probably due to flow separation at the wing tip. In the low Mach number range the addition of the fuselage had no effect on the lateral center of pressure, but at Mach numbers near 1.0 the magnitude of the over-all movement was appreciably reduced.

Pitching-Moment Characteristics

Near zero lift the wing-alone aerodynamic center $\left(\partial C_m/\partial C_L\right)_M$ was located on or near the quarter-chord point of the mean aerodynamic chord up to a Mach number of 0.90. This compared favorably with the value obtained at low speeds and high Reynolds number for the 6-percent-thick wing with identical plan form of reference 5 but was about 14 percent of

the mean aerodynamic chord farther forward than the value obtained from the transonic-bump investigation of the 6-percent-thick wing. (See reference 3.) Inasmuch as the lateral center of pressure was shown to be independent of wing thickness at Mach numbers below 0.90, the large aerodynamic-center difference may be attributable to a more rearward chordwise center-of-pressure location for the thinner wing at low Reynolds number which, in turn, may have been occasioned by leading-edge separation.

In the Mach number range between 0.95 and 1.15 the aforementioned loss of loading at the wing tip for low lift coefficients produced a large unstable movement in the wing aerodynamic center. There was no such effect observed for the 6-percent-thick wing of reference 3. As previously stated, the addition of the fuselage reduced the loading changes at high Mach numbers and this was reflected in the smaller aerodynamic-center change for the high Mach number range.

In the subsonic speed range, the wing-alone and the wing-fuselage pitching-moment curves indicated appreciable instability at the higher lift coefficients, but at the higher Mach numbers no instability was obtained for the range of lift coefficients tested. (See figs. 8 and 9.) A comparison of these data with those of reference 3 indicates that wing-thickness changes did not substantially alter the pitching-moment characteristics at higher lift coefficients.

Downwash and Dynamic Pressure

The downwash gradients $\left(\partial\epsilon/\partial\alpha\right)_M$ near zero lift for both wing-alone and wing-fuselage configurations were practically the same for all tail heights investigated up to about $M = 0.85$. (See figs. 12 and 14.) Above this Mach number the values of $\left(\partial\epsilon/\partial\alpha\right)_M$ for both wing-alone and wing-fuselage configurations were greatest for a tail height near the wing chord plane extended (zero tail height). The downwash gradients for the 9-percent-thick wing are similar to those of the 6-percent-thick wing of identical plan form (reference 3), particularly at Mach numbers below 0.85. For Mach numbers above 0.85 the thicker wing created higher downwash gradients in the vicinity of the chord plane extended.

The results of the point-dynamic-pressure surveys (fig. 13) showed that for the wing alone there were no important changes in the shape or magnitude of the wake with Mach number and that the addition of the fuselage had practically no effect on the dynamic-pressure ratios throughout the Mach number range investigated. For most of the Mach numbers the wake losses (maximum of about 8 or 9 percent at the highest Mach numbers) were about the same as those obtained for the thinner

[redacted]

wing (reference 3). However, for the highest Mach number and angles of attack, the total wake losses were slightly greater for the 9-percent-thick-wing configuration of this investigation.

Langley Aeronautical Laboratory
National Advisory Committee for Aeronautics
Langley Air Force Base, Va.

REFERENCES

1. Weil, Joseph, and Goodson, Kenneth W.: Aerodynamic Characteristics of a Wing with Quarter-Chord Line Swept Back 45°, Aspect Ratio 4, Taper Ratio 0.6, and an NACA 65A006 Airfoil Section. Transonic-Bump Method. NACA RM L9A21, 1949.

2. Myers, Boyd C., II, and King, Thomas J., Jr.: Aerodynamic Characteristics of a Wing with Quarter-Chord Line Swept Back 45°, Aspect Ratio 4, Taper Ratio 0.3, and NACA 65A006 Airfoil Section. Transonic-Bump Method. NACA RM L9E25, 1949.

3. Goodson, Kenneth W., and Few, Albert G., Jr.: Aerodynamic Characteristics of a Wing with Quarter-Chord Line Swept Back 45°, Aspect Ratio 6, Taper Ratio 0.6, and NACA 65A006 Airfoil Section. Transonic-Bump Method. NACA RM L9I08, 1949.

4. Schneiter, Leslie E., and Ziff, Howard L.: Preliminary Investigation of Spoiler Lateral Control on a 42° Sweptback Wing at Transonic Speeds. NACA RM L7F19, 1947.

5. Cahill, Jones F., and Gottlieb, Stanley M.: Low-Speed Aerodynamic Characteristics of a Series of Swept Wings Having NACA 65A006 Airfoil Sections. NACA RM L9J20, 1949.

[redacted]

TABLE I.- FUSELAGE ORDINATES

Basic fineness ratio 12; actual fineness ratio 10 achieved by cutting off the rear one-sixth of the body; $8/4$ located at $l/2$

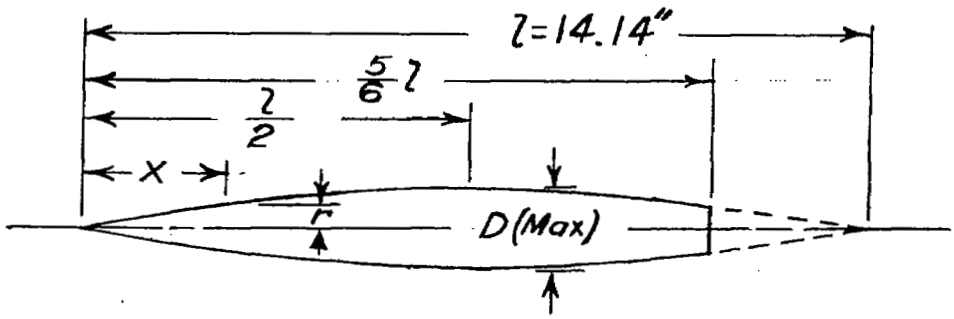

Ordinates			
x/l	r/l	x/l	r/l
0	0	0	0
.005	.00231	.4500	.04143
.0075	.00298	.5000	.04167
.0125	.00428	.5500	.04130
.0250	.00722	.6000	.04024
.0500	.01205	.6500	.03842
.0750	.01613	.7000	.03562
.1000	.01971	.7500	.03128
.1500	.02593	.8000	.02526
.2000	.03090	.8333	.02083
.2500	.03465	.8500	.01852
.3000	.03741	.9000	.01125
.3500	.03933	.9500	.00439
.4000	.04063	1.0000	0
L. E. radius = 0.0005l			

NACA

[redacted]

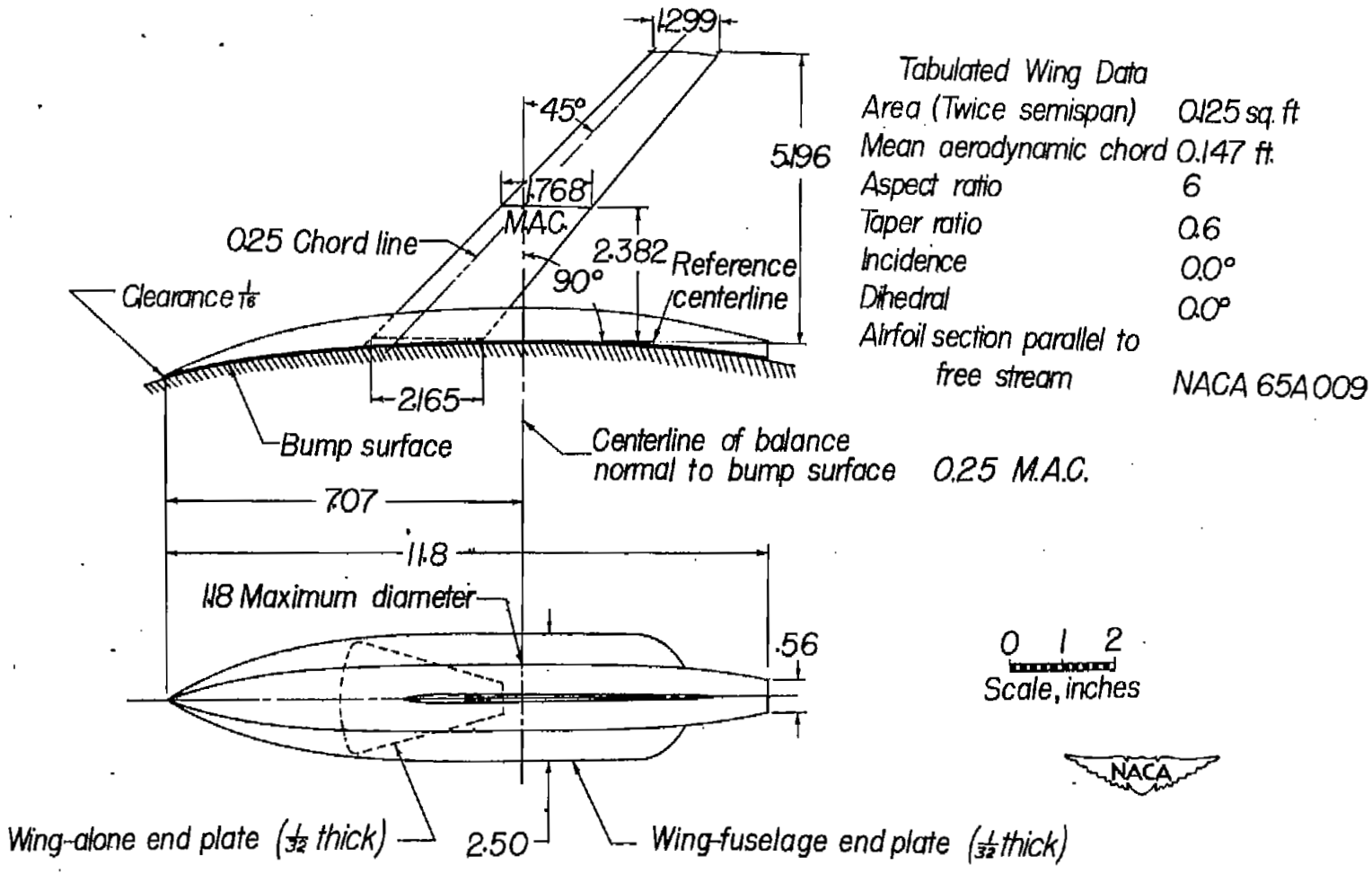

Tabulated Wing Data

Area (Twice semispan)	0.125 sq. ft
Mean aerodynamic chord	0.147 ft.
Aspect ratio	6
Taper ratio	0.6
Incidence	0.0°
Dihedral	0.0°
Airfoil section parallel to free stream	NACA 65A009

Figure 1.- General arrangement of a model with 45° sweptback wing, aspect ratio 6, taper ratio 0.6, and NACA 65A009 airfoil section.

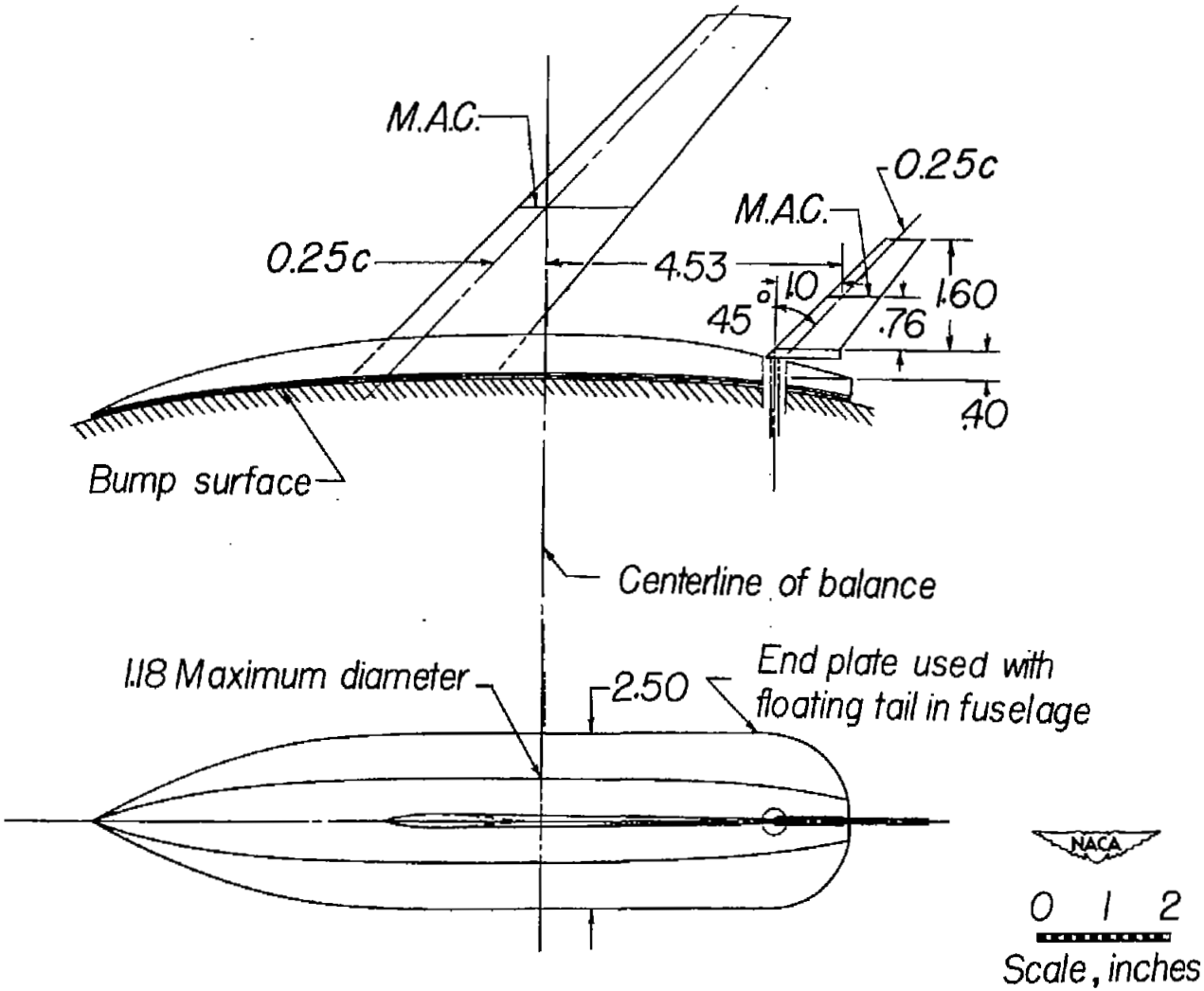

Figure 2.- Details of free-floating tail mounted in fuselage of a model with 45° sweptback wing, aspect ratio 6, taper ratio 0.6, and NACA 65A009 airfoil section.

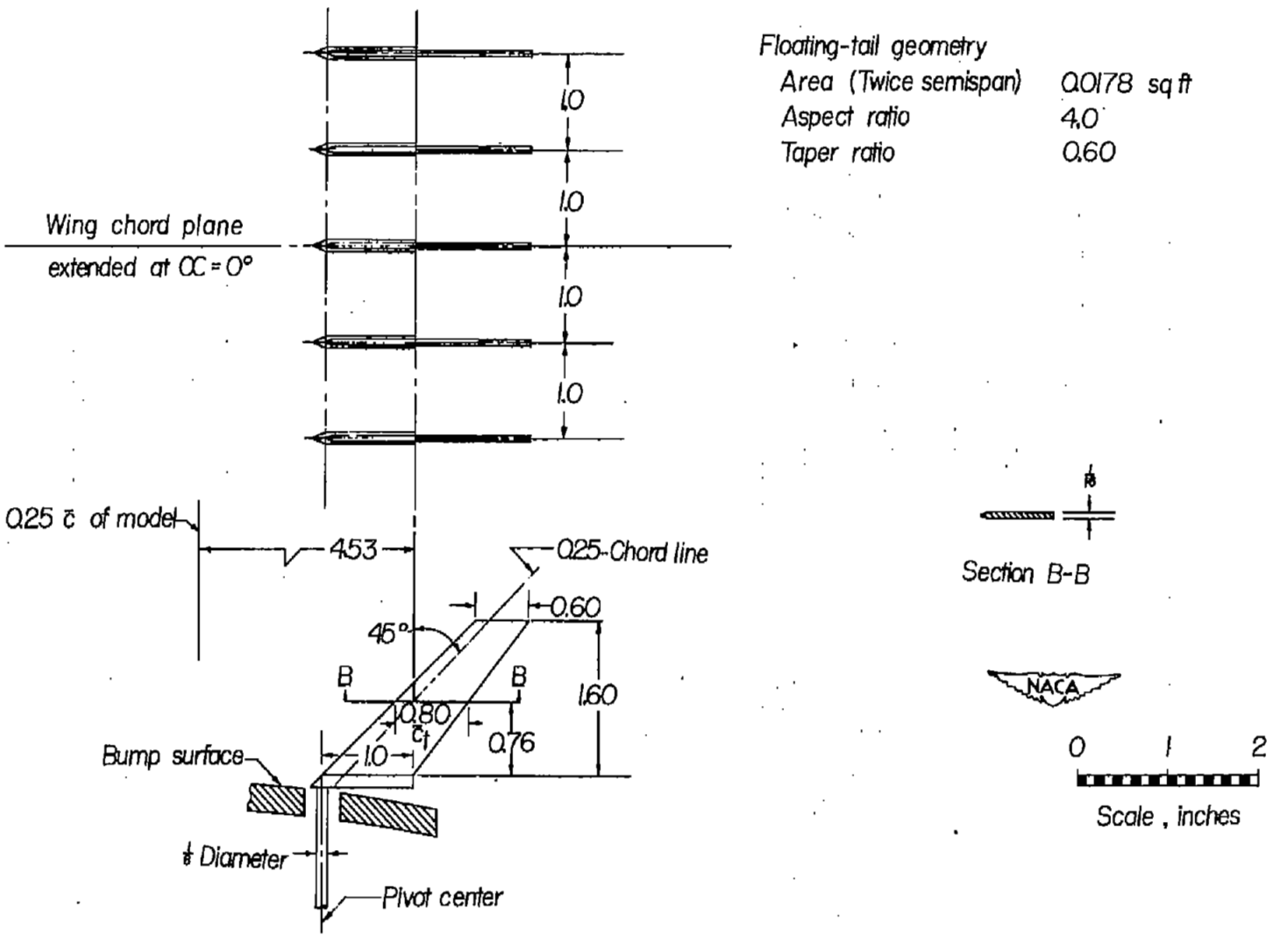

Figure 3.- Details of free-floating tails used in surveys behind model with 45° sweptback wing, aspect ratio 6, taper ratio 0.6, and NACA 65A009 airfoil. All dimensions are in inches.

Figure 4.- Photograph of a model with 45° sweptback wing, aspect ratio 6, taper ratio 0.6, and NACA 65A009 airfoil section mounted on the transonic bump showing free-floating tails.

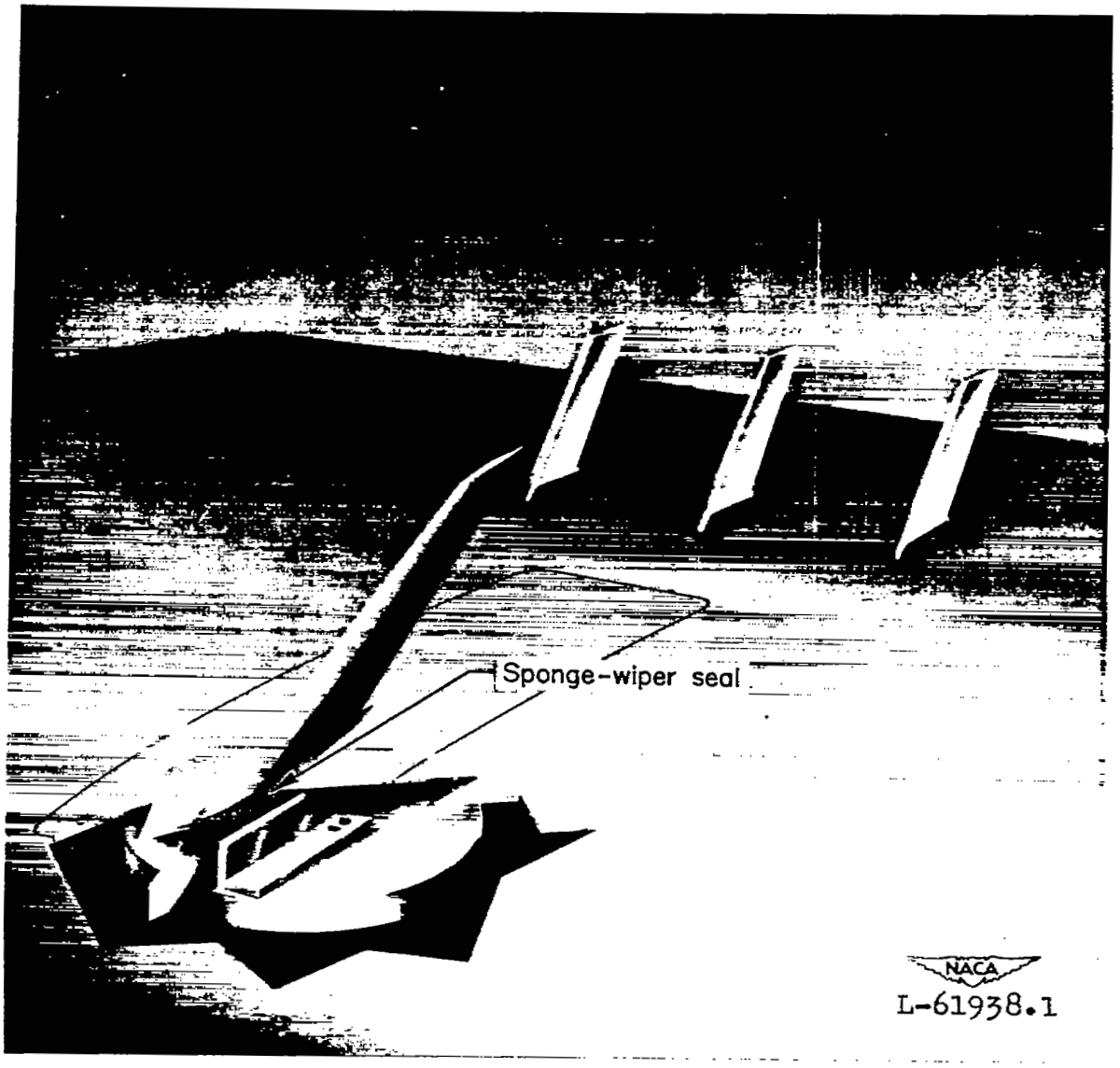

Figure 5.- Pictorial view showing the sponge-wiper seal installed on the model.

[redacted]

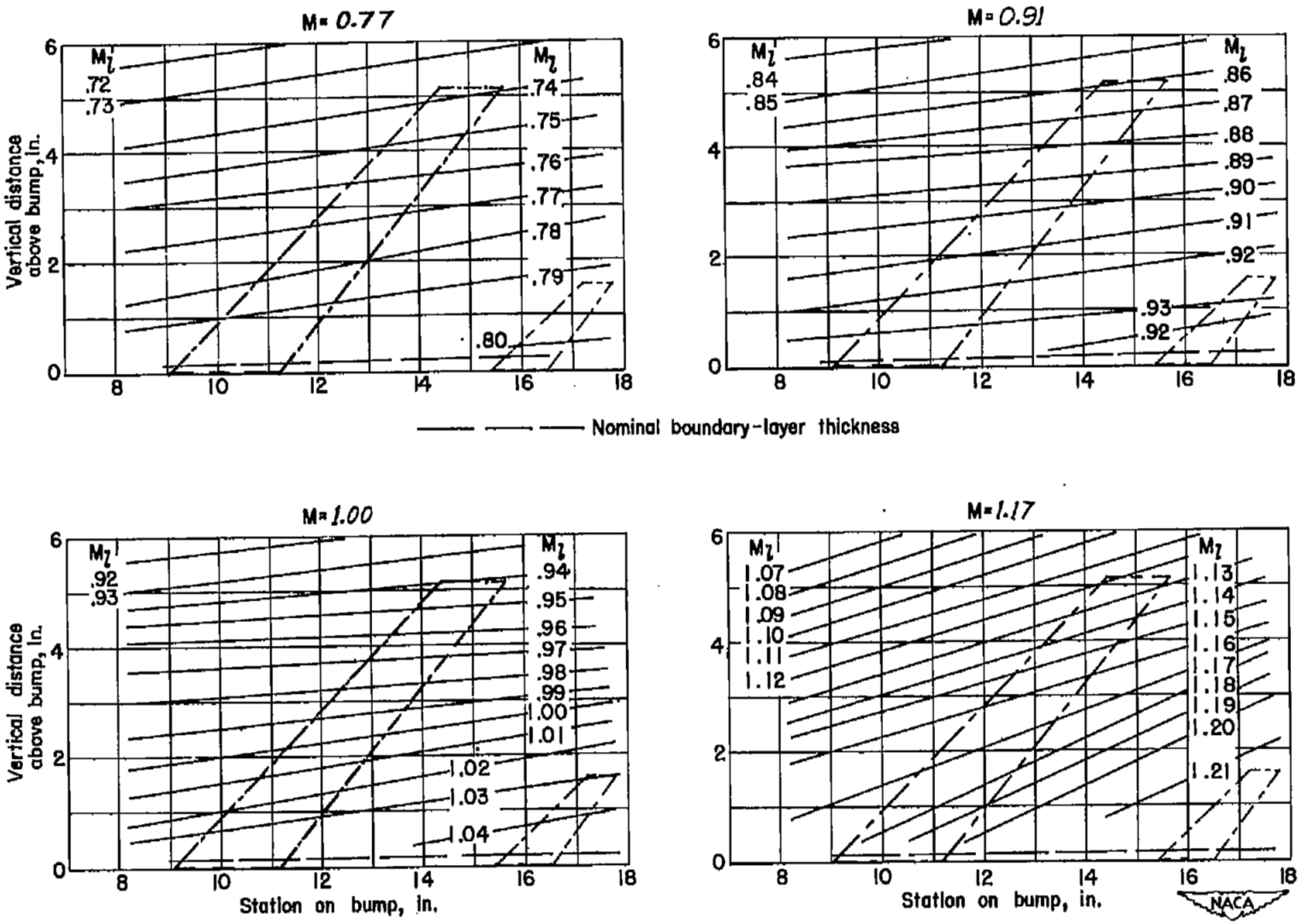

Figure 6.- Typical Mach number contours over transonic bump in region of model location.

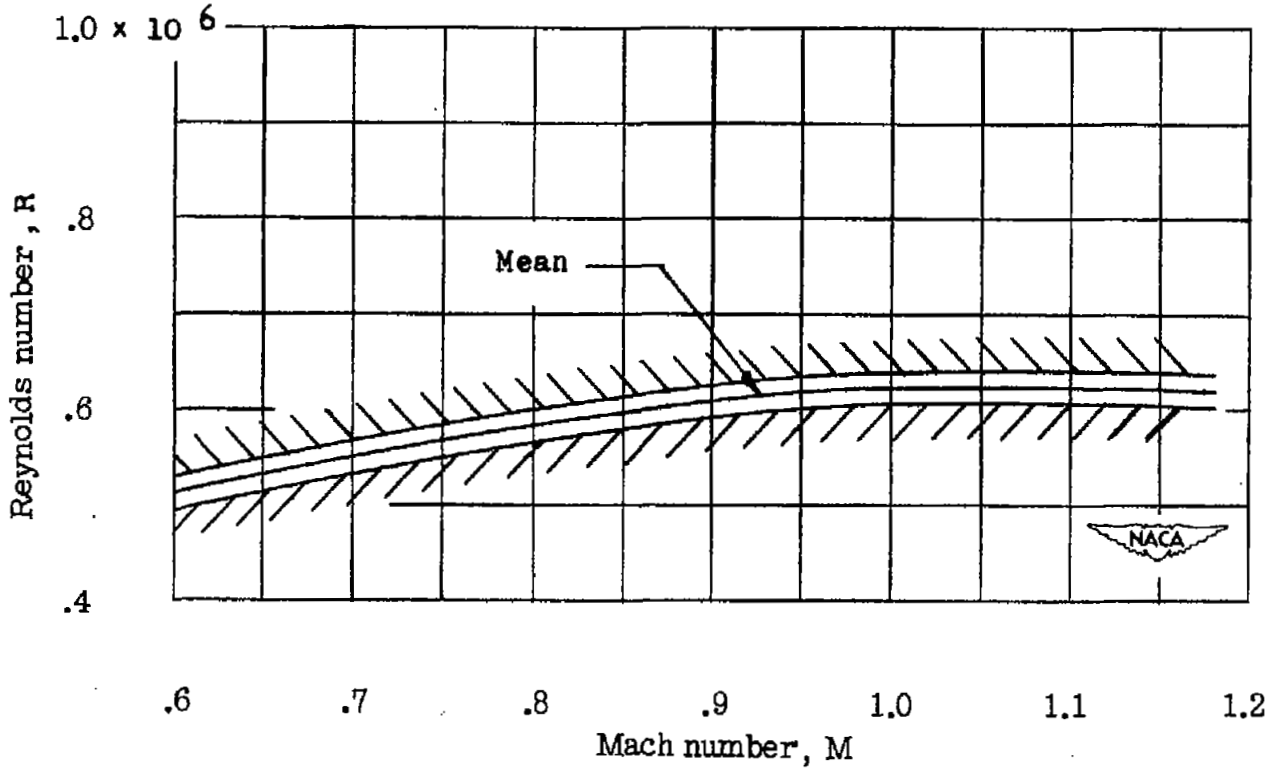

Figure 7.- Variation of test Reynolds number with Mach number for a model with 45° sweptback wing, aspect ratio 6, taper ratio 0.6, and NACA 65A009 airfoil section.

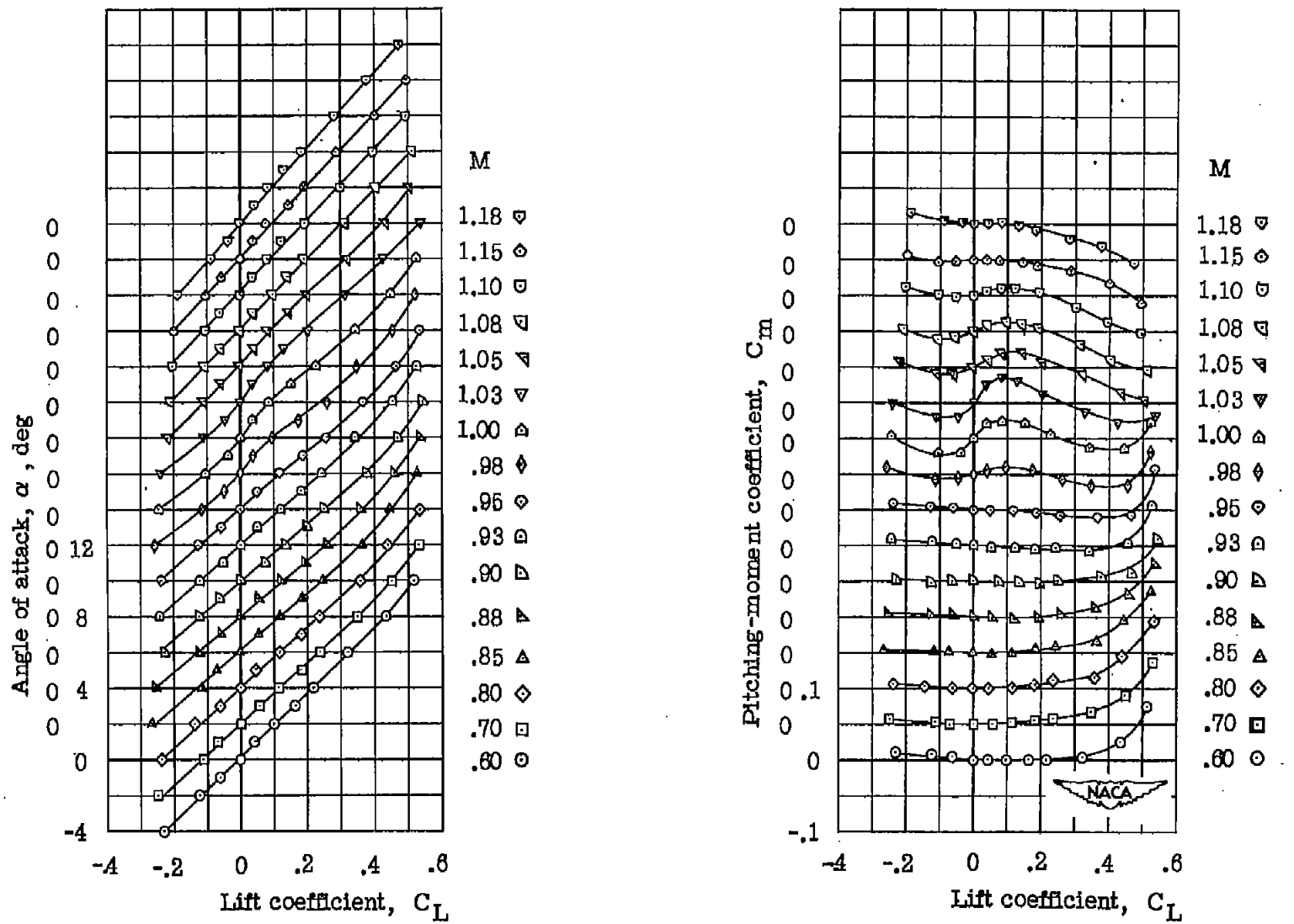

Figure 8.- Wing-alone aerodynamic characteristics for a model with 45° sweptback wing, aspect ratio 6, taper ratio 0.6, and NACA 65A009 airfoil section.

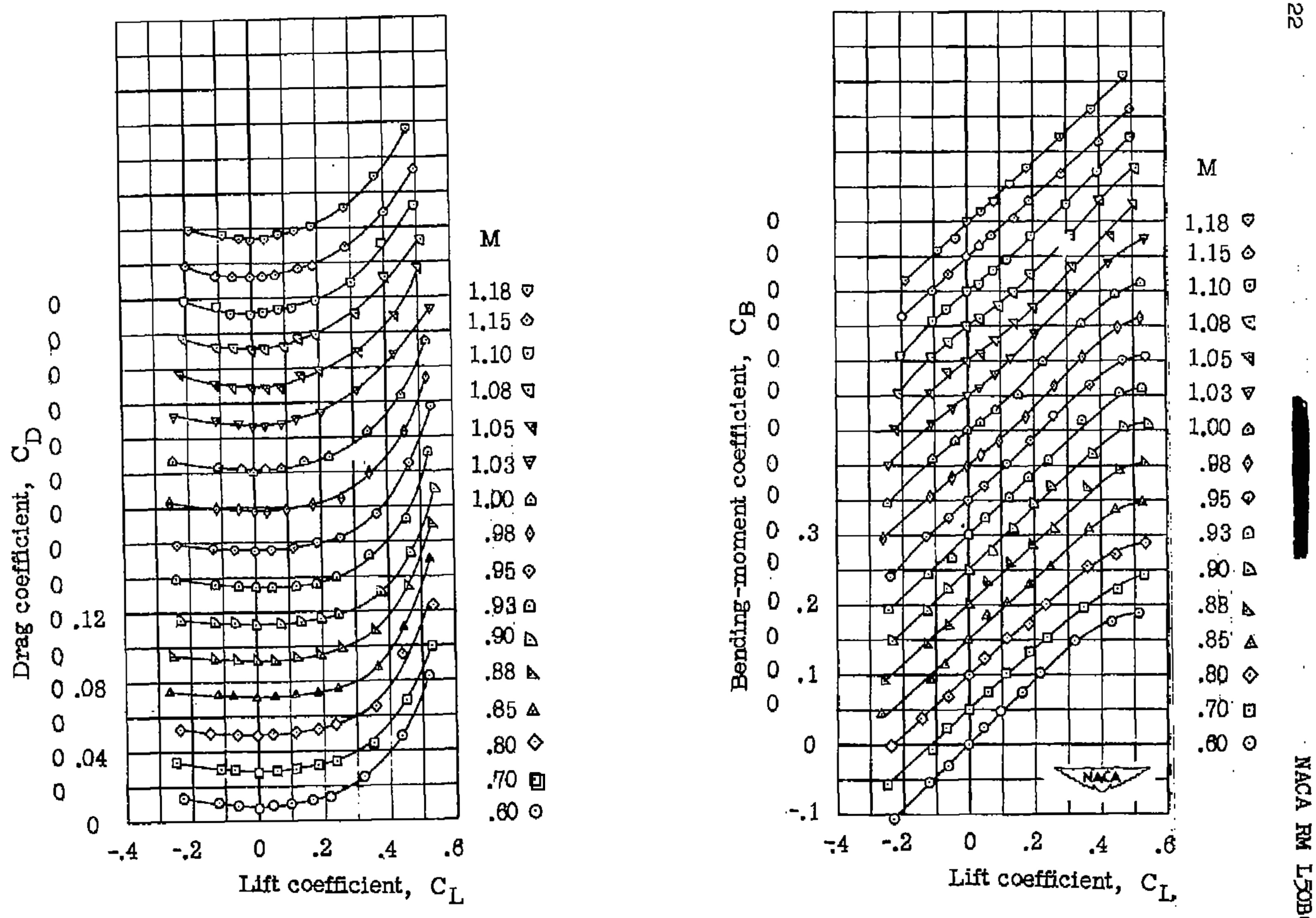

Figure 8.- Concluded.

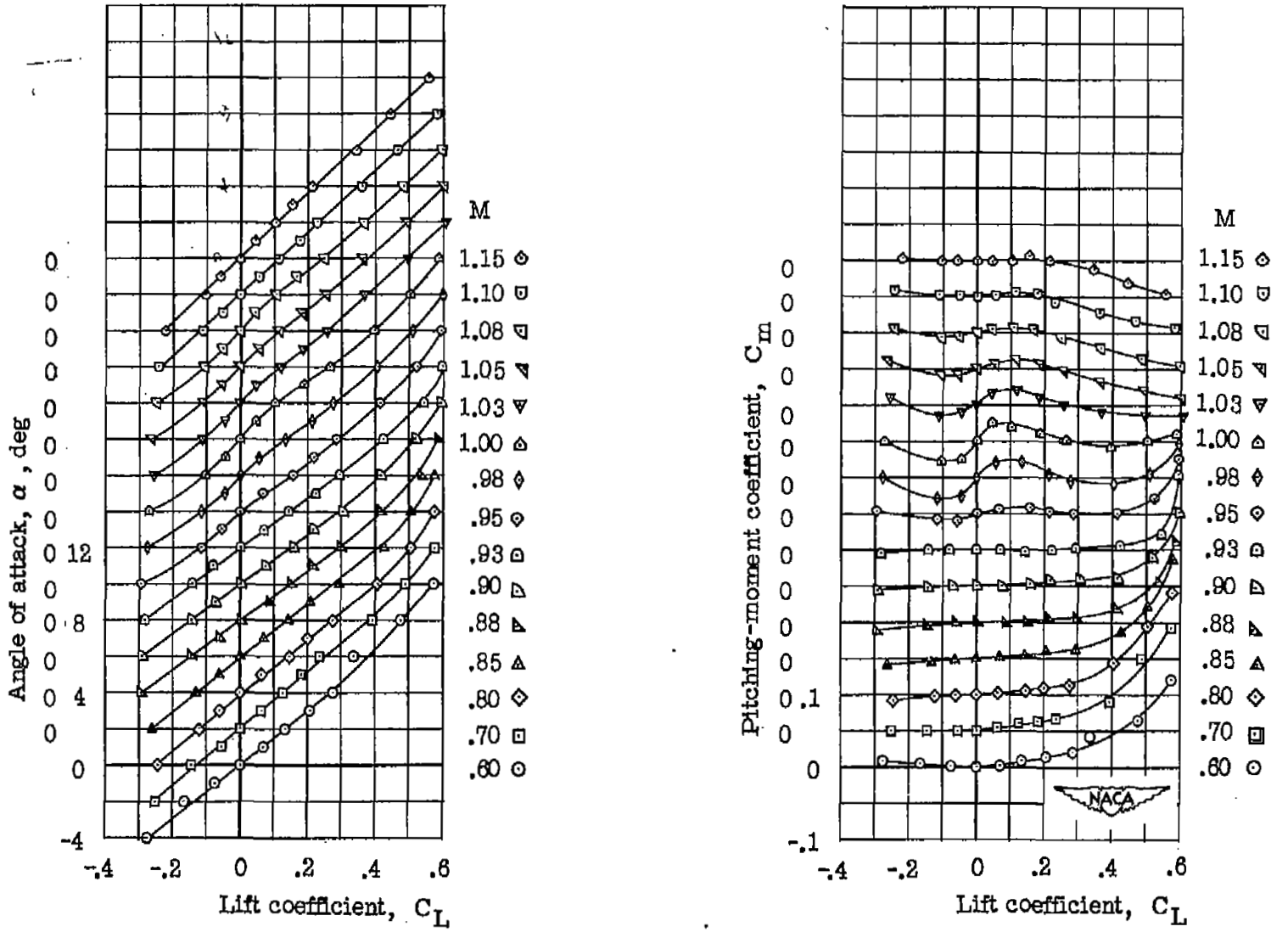

Figure 9.- Wing-fuselage aerodynamic characteristics for a model with 45° sweptback wing, aspect ratio 6, taper ratio 0.6, and NACA 65A009 airfoil section.

[redacted]

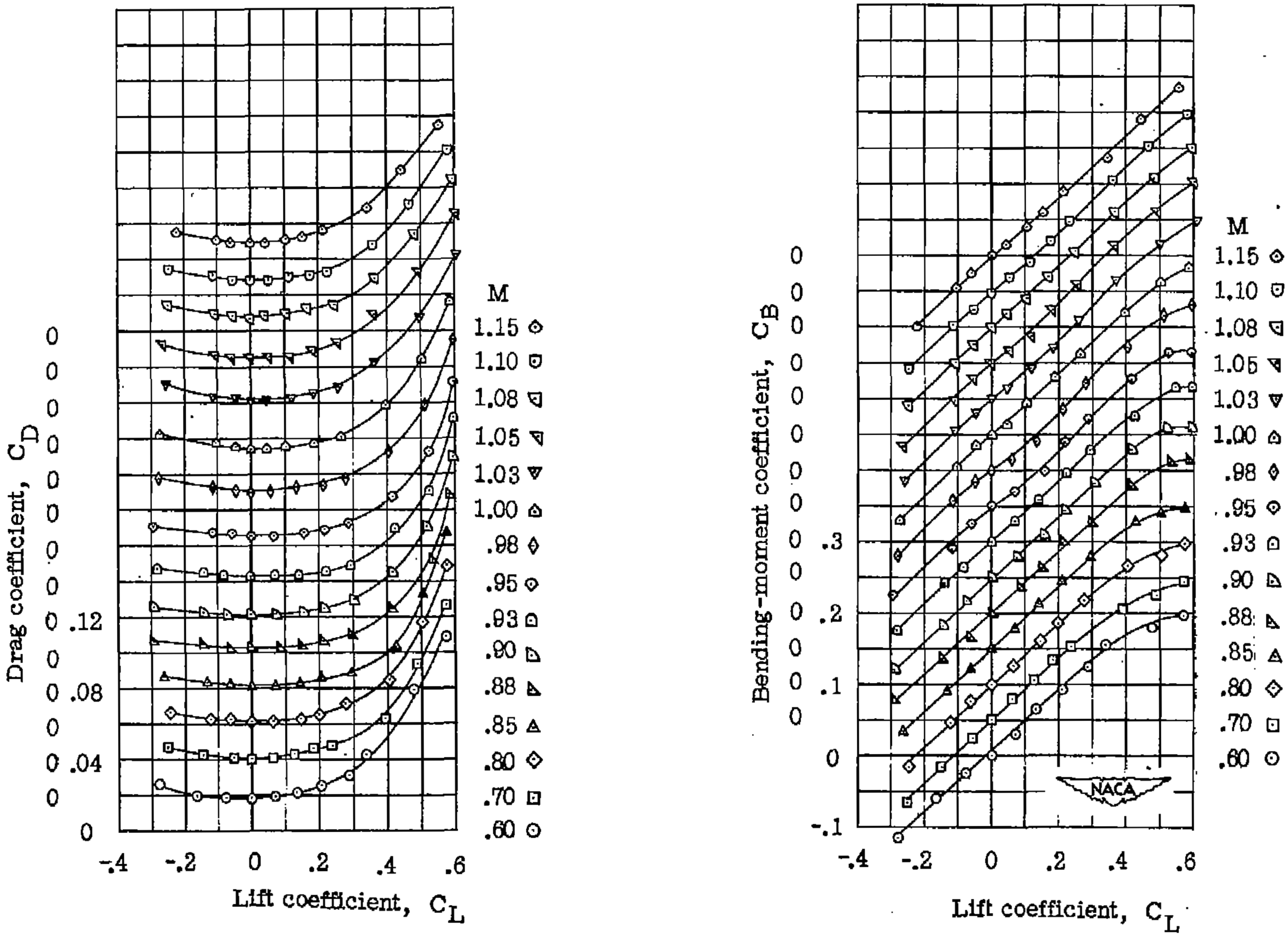

[redacted]

Figure 9.- Concluded.

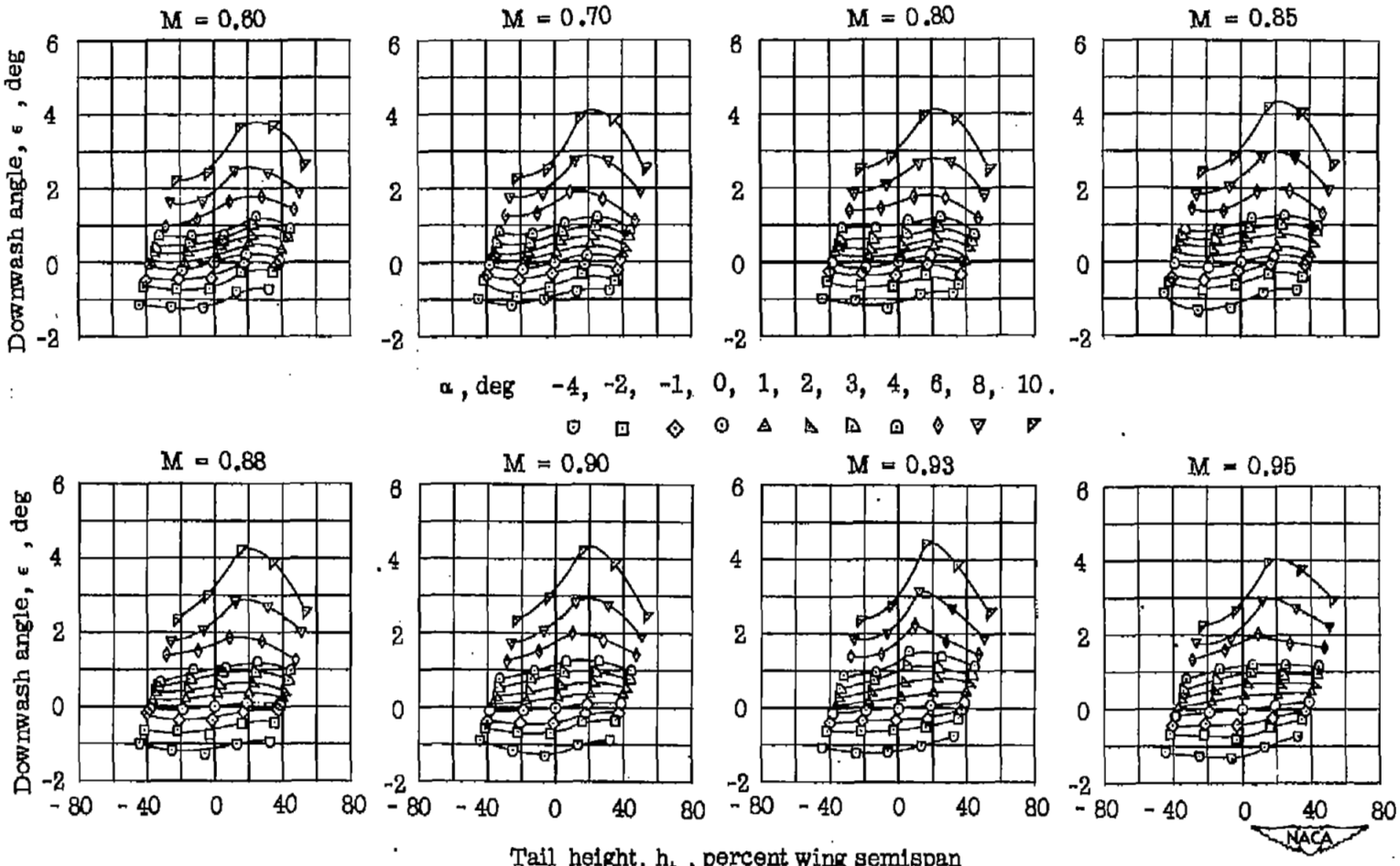

Figure 10.- Effective downwash angles in region of tail plane for a model with 45° sweptback wing, aspect ratio 6, taper ratio 0.6, and NACA 65A009 airfoil section. Wing-alone.

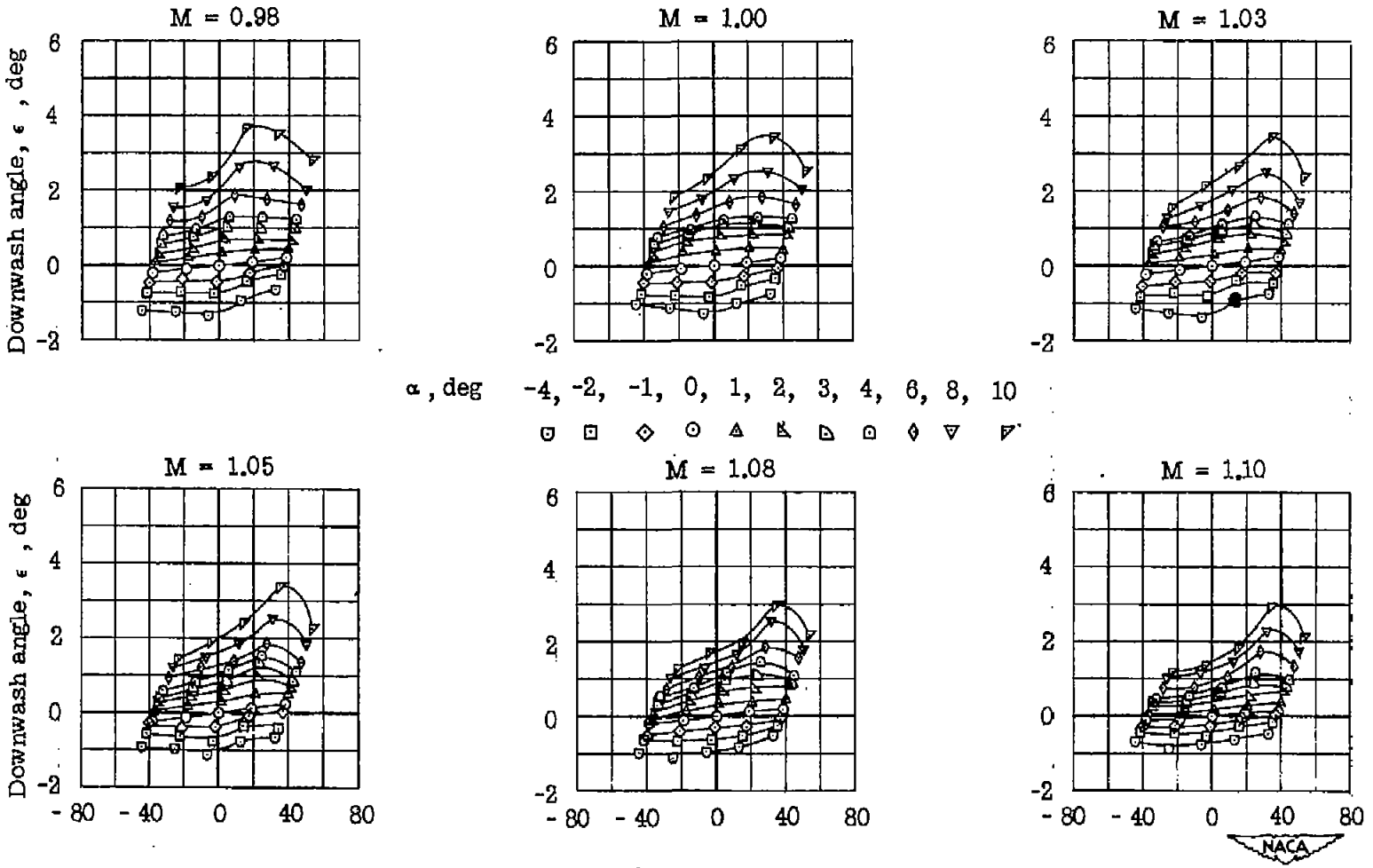

Figure 10.- Concluded.

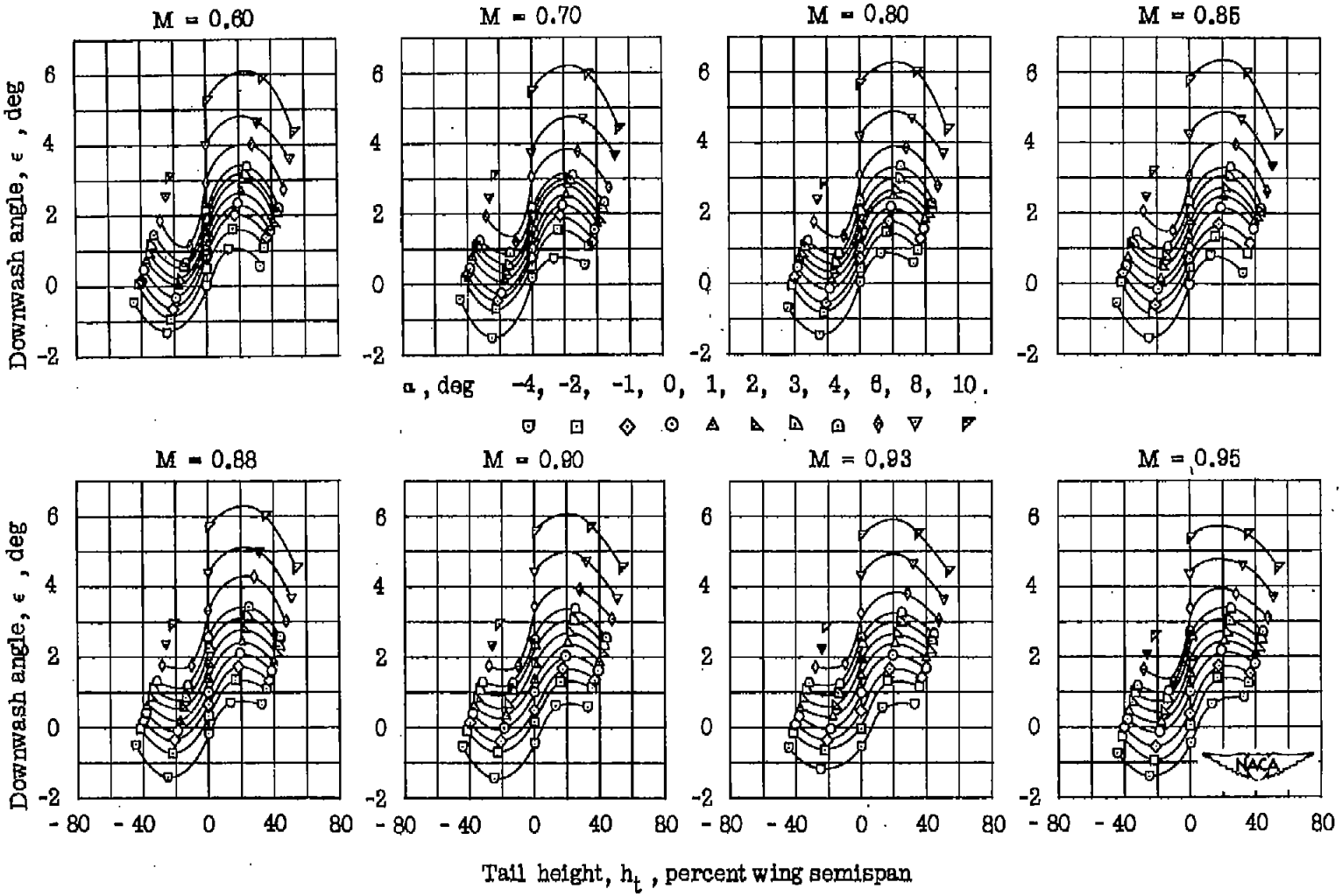

Figure 11.- Effective downwash angles in region of tail plane for a model with 45° sweptback wing, aspect ratio 6, taper ratio 0.6, and NACA 65A009 airfoil section. Wing-fuselage.

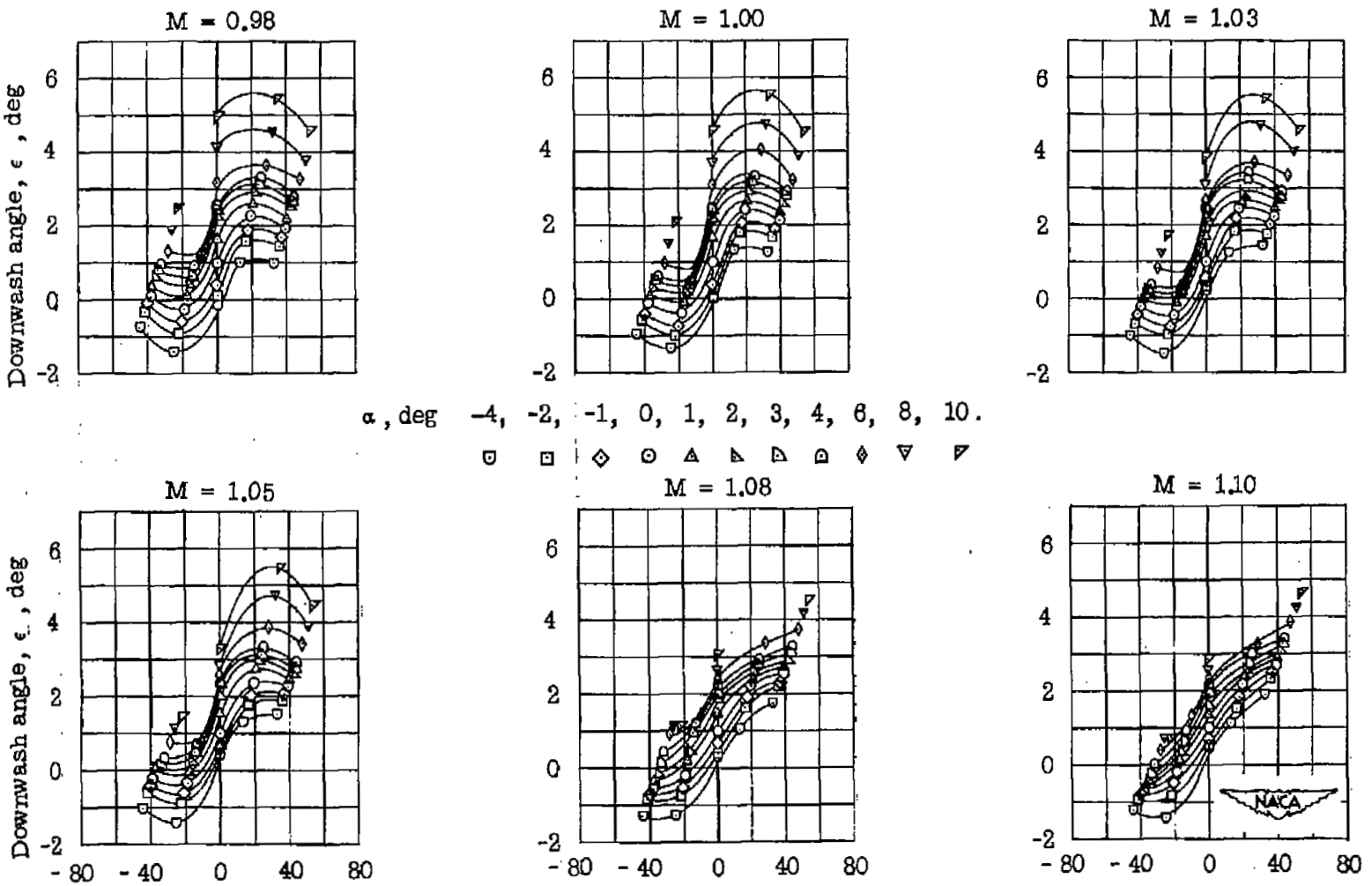

Figure 11.- Concluded.

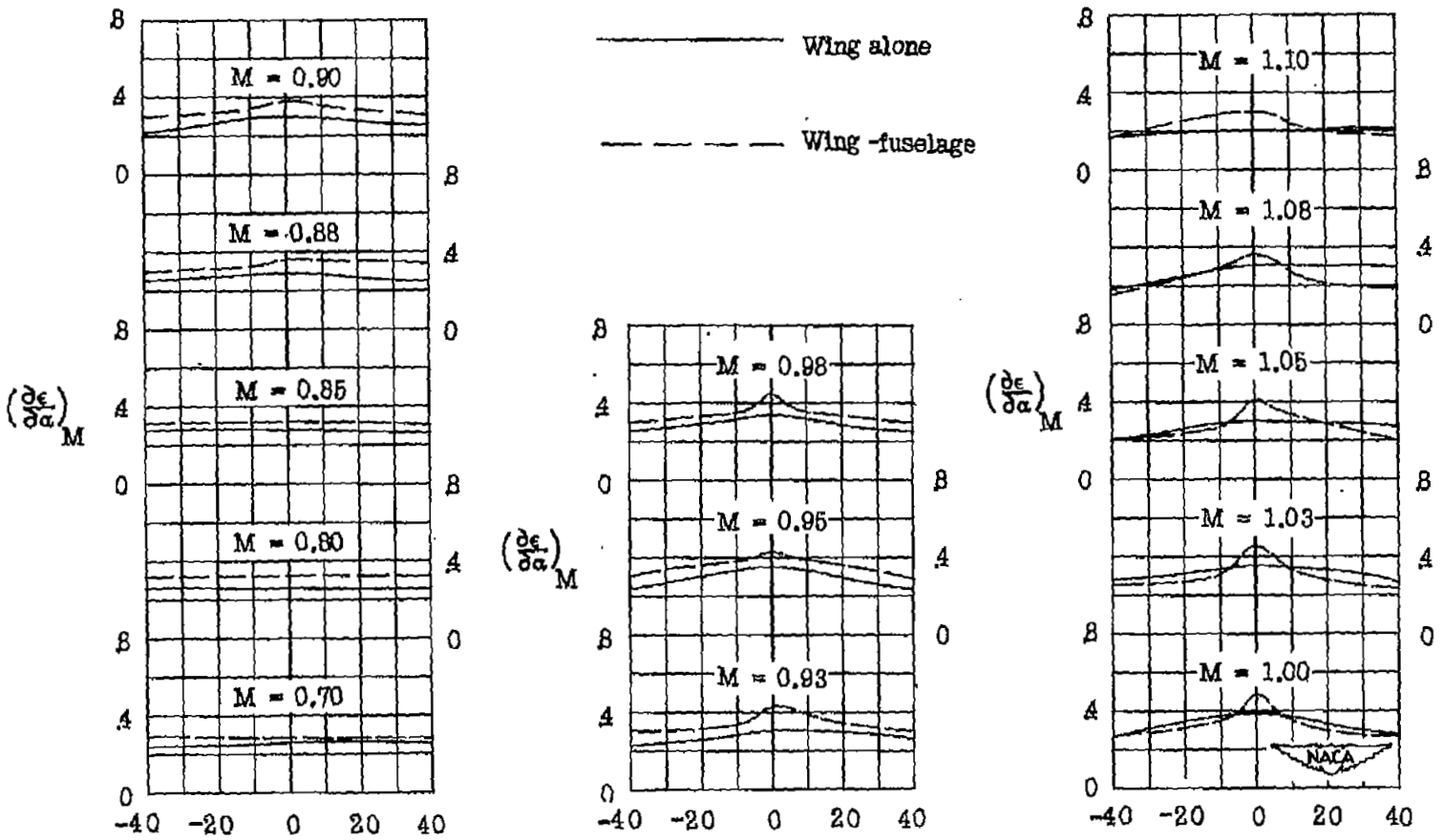

Figure 12.- Variation of downwash gradient with tail height and Mach number for a model with 45° swept-back wing, aspect ratio 6, taper ratio 0.6, and NACA 65A009 airfoil section. ($C_L = 0$)

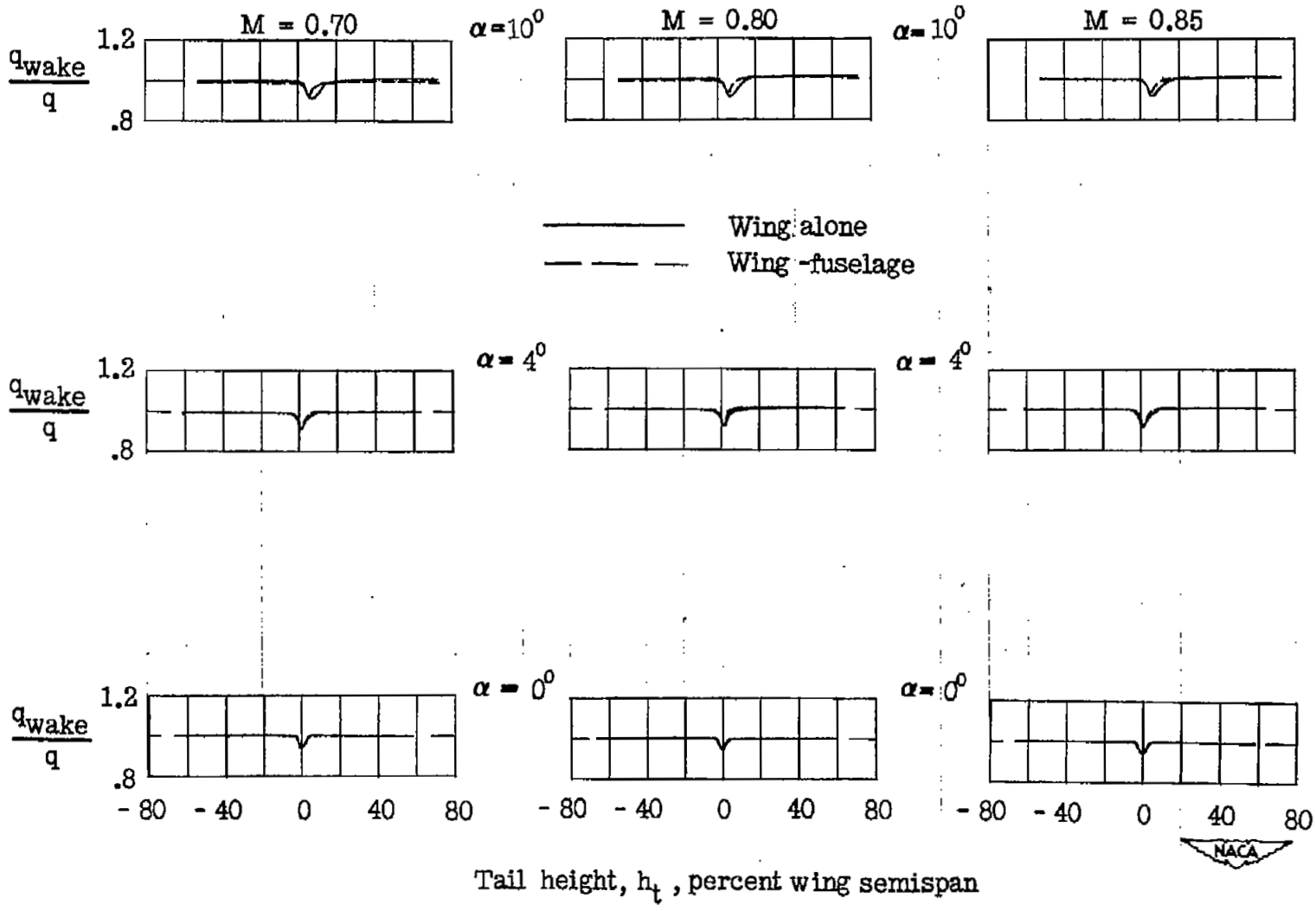

Figure 13.- Dynamic pressure surveys in region of tail plane for a model with 45° sweptback wing, aspect ratio 6, taper ratio 0.6, and NACA 65A009 airfoil section.

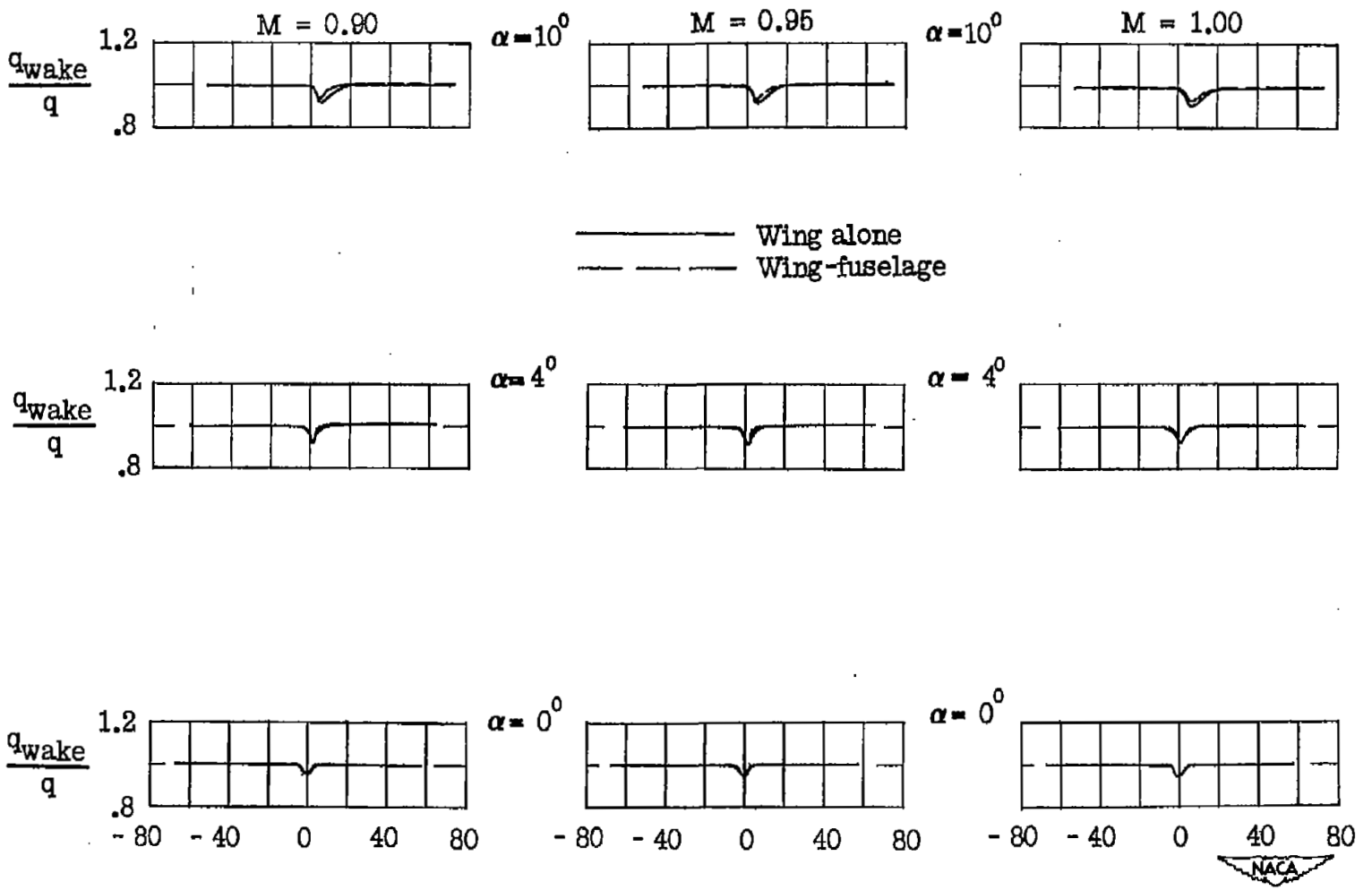

Tail height, h_t, percent wing semispan

Figure 13.- Continued.

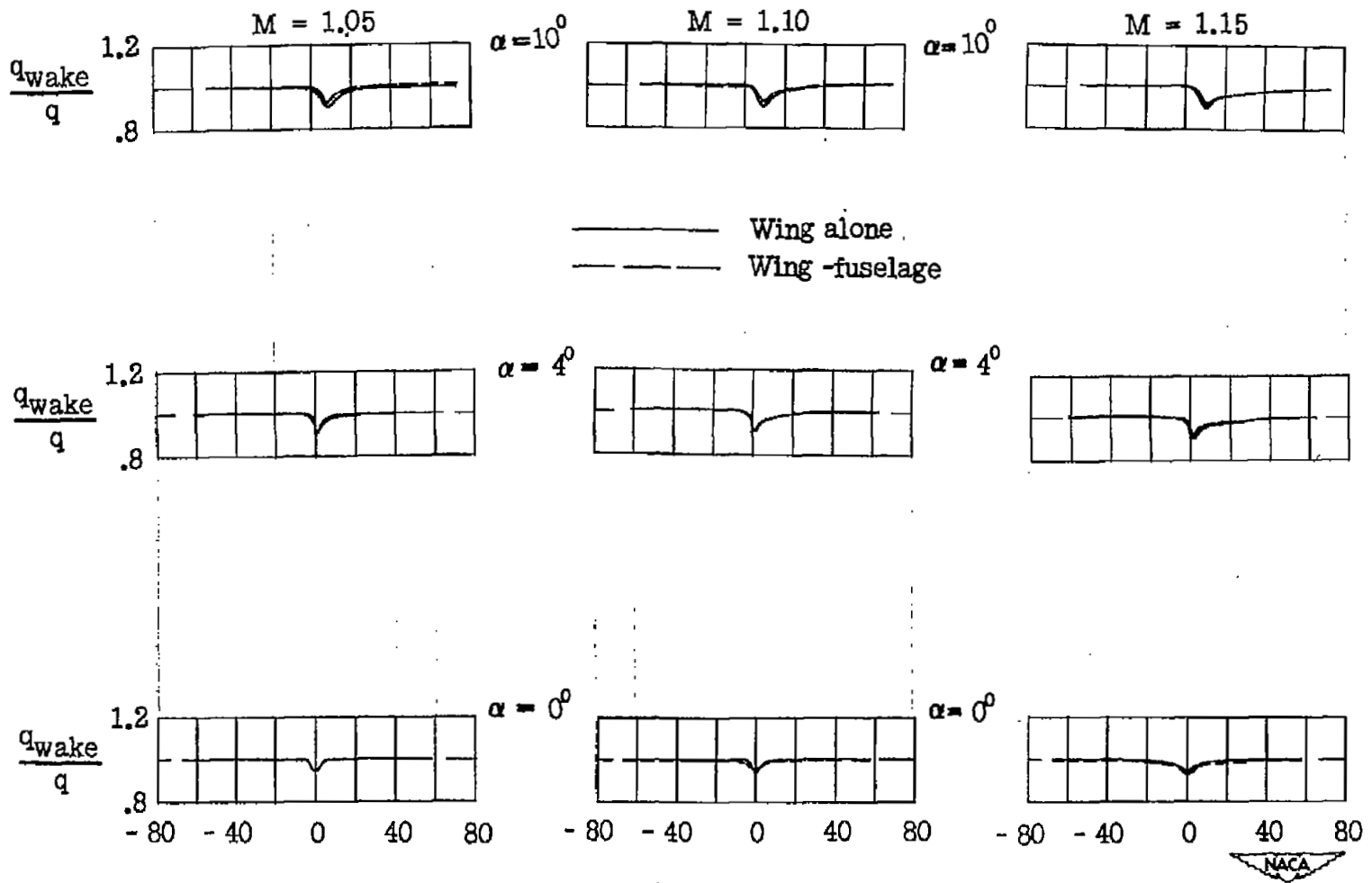

Figure 13.- Concluded.

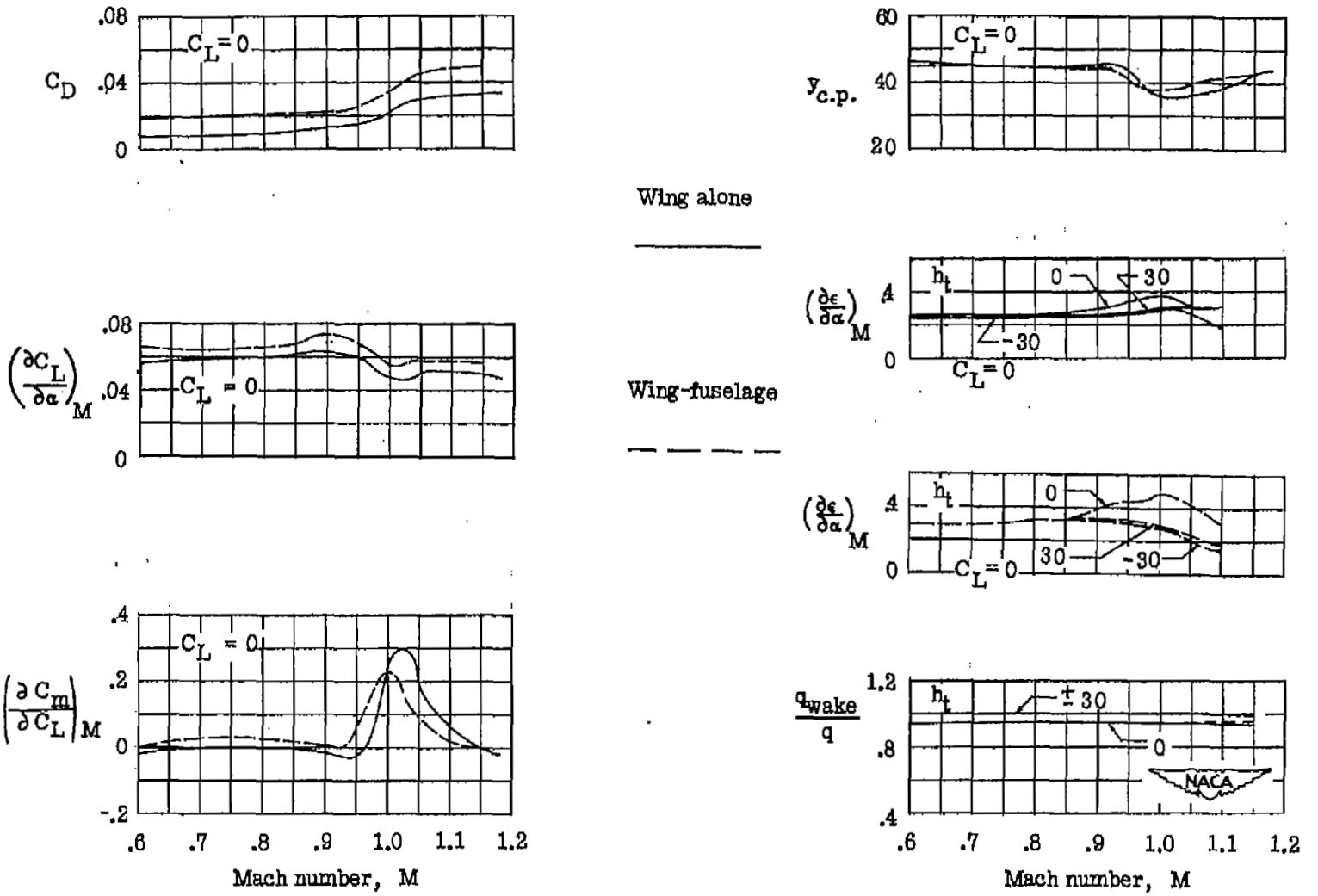

Figure 14.- Summary of aerodynamic characteristics for a model with 45° sweptback wing, aspect ratio 6, taper ratio 0.6, and NACA 65A009 airfoil section.